RSC Advances

ROYAL SOCIETY OF CHEMISTRY

www.rsc.org/advances

Cite this: DOI: 10.1039/c0xx00000x

www.rsc.org/xxxxxx

ARTICLE TYPE

Synthesis of high purity chain-like carbon nanospheres in ultrahigh yield, and their microwave absorption prperties

Xiaosi Qi,[a,b] Jianle Xu,[a] Wei Zhong,*[,b] Youwei Du[b]

Received (in XXX, XXX) Xth XXXXXXXXX 20XX, Accepted Xth XXXXXXXXX 20XX

DOI: 10.1039/b000000x

Abstract: Over Fe/SnO_2 nanoparticles generated by a combined sol-gel/reduction method, high purity chain-like carbon nanospheres (CNSs) could be synthesized in large quantities through the catalytic decomposition of acetylene at 700 °C. The effect of SnO_2 content on the yield, microstructure and microwave absorbing properties of the obtained CNSs were studied in detail. The results demonstrate that the content of SnO_2 has a great impact on the yield and dimension of the obtained CNSs, and ultrahigh yield of 309 was reported. Moreover, the smaller size of chain-like CNSs, which can be obtained over the catalysts with higher SnO_2 content, exhibit enhanced microwave absorption properties due to their better complementarities between the dielectric and magnetic tangent loss. Based on the results, we also discuss the possible formation mechanism of CNSs. Therefore, we propose a simple and environment-friendly route for the mass production of chain-like CNSs with high purity, and the as-synthesized chain-like CNSs exhibit good microwave absorbing ability.

Keywords: Carbon materials; chemical vapor deposition; microwave absorption property

1. Introduction

In the last two decades, many researchers have focused their interest in the study of carbon nanotubes (CNTs), carbon nanofibers (CNFs) and fullerene because of their excellent properties and potential applications in more and more fields [1-3]. It is well known that carbon, as an element, is unique in the number and the variety of ways in which it can bond. Apart from the filamentous arranges of graphene sheets conducting to CNT or CNF, the paring of pentagonal, heptagonal and hexagonal carbon rings can also arrange to create novel structures with dissimilar properties [4]. Among those novel structures, because of their unclosed sheets in the spherical arrangement, carbon nanospheres (CNSs) have only started to attract considerable attention in recent years. The unclosed graphitic flakes of CNSs can create many open edges at the surface and provide reactive "dangling bonds", which enhance surface reactions and establish their excellent properties and potential applications in the fields of gas storage, sensing, lithium-ion batteries, adsorption and so on [5-7]. It is thus very desiderative to exploit simple and reliable processes to produce this new carbon material. Generally, the present methods for CNS synthesis involve hydrothermal reaction, arc plasma technique, metathesis reaction and template route [8-11]. The aforementioned methods for synthesizing CNSs still suffer from low product yields and purities, which limit their use in these applications greatly.

Catalytic chemical vapor deposition (CCVD), as a promising technique for the growth of carbon nanomaterials (CNMs), has several advantages including high selectivity, high yield, low cost and selective growth [12-14]. However, the reported yield and/or purity of CNSs produced through CVD process was typical low, and the size of as-synthesized CNSs had a wide distribution [15-17].

Recently, the microwave absorbing performance of various structured CNMs such as CNTs, helical carbon nanomaterials (HCNMs), etc. have been investigated intensively for the possible applications as effective and lightweight electromagnetic (EM) irradiation shielding materials [18-20]. However, the study of CNSs as the microwave absorber in the open literature is seldom. Enlightened by the merit of the previous work [21], we believe that SnO_2 plays an important role on the formation and yield of the obtained CNSs. In this work, we report the large-scale synthesis of well-defined chain-like CNSs with the assistance of SnO_2 and attempt to investigate electromagnetic, microwave absorbing properties and possible formation mechanism of the obtained chain-like CNSs.

2. Experimental

2.1 Synthesis of Catalyst Precursor.

Similar to the method reported elsewhere [22], in a typical experiment, 0.03 mol $FeCl_2{\cdot}4H_2O$ and 0.045 mol citric acid monohydrate were dissolved in 200 ml absolute ethanol. After stirred at 60 °C for 6 h, a clear solution was obtained. Then amount of $SnCl_4{\cdot}5H_2O$ (0.0015 mol) was added to the solution, and the mixture was stirred for 2 h. The resulting mixture was kept at 80 °C until the formation of a xerogel. After heating the xerogel in air at 500 °C for 4 h, the catalyst precursor (denoted as No. 1) was obtained. By a similar approach, No. 2 and 3 catalyst precursors were generated using 0.0045 and 0.0100 mol

$SnCl_4 \cdot 5H_2O$ with other experimental conditions unchanged, respectively.

2.2 Synthesis of Chains-like CNSs.

In this process, 0.03 g of the catalyst precursor powder was dispersed on a ceramic plate which was then placed inside a quartz reaction tube (60 cm in inner diameter and 100 cm in length). Firstly, the temperature of furnace was raised from room temperature (RT) to 500 °C in Ar for 1 h. Then, the corresponding catalyst precursor powder was in situ reduced in H_2 at 500 °C for 4 h. After that, the temperature of furnace was raised from 500 to 700 °C in Ar for 0.5 h. Finally, Ar was cut off and acetylene was introduced into the tube at 700 °C for 4 h. After cooling to RT with Ar flowing through the reaction tube, large quantities of black powder (denoted as A, B and C) were collected, respectively.

2.3 Characterization of products.

The phases and morphologies of sample were examined over an X-ray powder diffractometer (XRD), transmission electron microscope (TEM), and field-emission scanning electron microscope (FE-SEM), respectively. Raman spectroscopic investigation was performed using a Jobin-Yvon Labram HR800 instrument with 514.5 nm Ar^+ laser excitation. For microwave measurement, 40 wt% of the as-prepared samples (A, B and C) and paraffin were mixed in a ceramic plate and stirred fully at 60 °C to give Composites A, B and C, respectively. And each composite was pressed into coaxial clapper in a dimension of outer diameter of 7.0 mm, inner diameter of 3.0 mm. The relative complex permittivity $(\varepsilon_r = \varepsilon_r' - j\varepsilon_r'')$ and permeability $(\mu_r = \mu_r' - j\mu_r'')$ of the composite were measured in frequency range of 2-18 GHz over an Agilent E8363B vector network analyzer. The reflection loss (RL) and attenuation constant (α) were calculated by the following equation:

$$RL = 20 \log \left| \frac{Z_{in} - 1}{Z_{in} + 1} \right| \quad (1)$$

$$Z_{in} = \sqrt{\frac{\mu_r}{\varepsilon_r}} \tanh\left(j \frac{2\pi f d \sqrt{\mu_r \varepsilon_r}}{c} \right) \quad (2)$$

$$\alpha = \frac{\sqrt{2}\pi f}{c} \sqrt{(\mu''\varepsilon'' - \mu'\varepsilon') + \sqrt{(\mu''\varepsilon'' - \mu'\varepsilon')^2 + (\varepsilon'\mu'' + \varepsilon''\mu')^2}} \quad (3)$$

where f is the frequency of EM wave, d is the thickness of absorber, c is the velocity of light and Z_{in} is the input impedance of absorber.

3. Results and discussion

3.1 XRD patterns of as-synthesized catalyst and sample.

For the catalytic growth of CNMs, the catalyst precursor was reduced in hydrogen to produce the corresponding catalyst (No. 1, 2 and 3). Figure 1 gives the XRD patterns of the as-synthesized No. 1 catalyst precursor and the corresponding catalyst. The XRD pattern of the as-prepared catalyst precursor (as shown in Figure 1a) shows that all the peaks can be indexed to Fe_2O_3, which is very close to the literature value (JCPDS No.85-0550). No other peaks of impurity can be detected. The XRD pattern of the obtained catalyst (No. 1) is shown in Figure 1b. One can see that all the strong and sharp peaks can be readily assigned to the cubic structure of Fe (JCPDS No.85-1410). Importantly, no impurity phases corresponding to ferric oxide such as Fe_2O_3 or Fe_3O_4 were observed, which should be related to the good protection of SnO_2 as the shell. The XRD result indicates that the as-synthesized catalyst is single phase Fe/SnO_2, which is consistent with that reported before [21]. As shown in Table 1, one can find that large quantities of samples can be obtained over the Fe/SnO_2 catalysts and the SnO_2 content has a greatly impact on the yield of the obtained sample. Similar results were reported before [23-25]. It is worth mentioning that the ultrahigh yield (209 and 309) of the desired product is a determining factor for its wide utilization. Compared to the ultrahigh yield of CNMs reported elsewhere [26], the CNM yield obtained here is high. And the ultrahigh yield of carbon species (309) was not reported before. In order to confirm the high yield of the obtained sample, four separate experiments were repeated. As shown in Figure 2, the proposed route shows a good reproducibility and is effective for the mass production of CNMs.

3.2 Microstructures, EM and microwave-absorbing properties of samples A, B and C.

Figure 3 gives the FE-SEM images and Raman spectrum of the obtained sample A. As shown in Figures 3a and b, the different magnifications of FE-SEM images reveal that the obtained sample A is chain-like spheroidal carbon particles, and the content (determined statistically by the FE-SEM observation) of such structure is up to 98%. It is apparent that these chain-like spheres have very uniform size and their average diameter is ca. 500 nm. According to the classification given by Serp et al. [27], the obtained carbon material in the case is called chain-like CNSs. Compared to those reported elsewhere [10,15-17], the route is simple and environment-friendly, and high purity uniform CNSs can be produced in ultrahigh yield here. Figure 3c presents the Raman spectrum of sample A. Two main broad peaks at ~1334 cm^{-1} named as D band for disordered graphite and ~1600 cm^{-1} called as G band for graphite carbon can be observed clearly [28,29]. The intensity ratio of G and D bands (I_G/I_D) is often used to identify the crystallinity of graphite. In the study, an I_G/I_D of ca. 1.21 was obtained for sample A. Compared to those of CNMs reported before [30,31], the I_G/I_D value of CNSs here is large, which implying high crystallinity of the obtained chain-like CNSs.

Figure 4 shows the variations of complex permittivity and permeability, loss tangent of Composite A with frequency. As illustrated in Figure 4a, with fluctuations during the low frequency range, the real (ε') and imaginary (ε'') part of relative complex permittivity almost remains constant, indicating that they have stable dielectric loss property. Figure 4b shows the real (μ') and imaginary (μ'') part of complex permeability as a function of frequency. One can see that the former is close to 1.17 while the latter to 0.05. It is worthy noted that the negative value of μ'' can be observed in the measured data (as shown in Figure 4b). There are three typical explanations about it worth noting: (i) the phenomenon can be explained by the magnetic energy being radiated out; (ii) it is meaningless and might be due to noise; (iii) the negative value is ascribed to the permeability-to-permittivity transform of EM wave in nanocomposites [32-37]. Based on the data in Figures 4a and b, the dielectric tangent ($\tan\delta_E = \varepsilon''/\varepsilon'$) and magnetic tangent loss ($\tan\delta_m = \mu''/\mu'$) are shown in Figure 4c. The $\tan\delta_E$ values are much larger than those of $\tan\delta_m$ in the

whole frequency range, indicating that the dielectric loss plays the main role in the EM absorption. Besides, one can observe clearly that the dielectric and magnetic loss have good complementarities, which is conducive to have a strong EM attenuation.

According to Eqs. (1) and (2), the RL value of the obtained composite was calculated, and the results are shown in Figure 5. As shown in Figure 5a, one can see that the RL value reaches maximum (-12.8 dB) at 8.4 GHz with a matching thickness (d_m) of 2.0 mm, and RL value below -10 dB (90% of EM wave attenuation) can be obtained in the 6.9-18 GHz frequency range with the sample thickness varied from 0.8 to 2.5 mm (as shown in Figure 5b). Compared to those of carbonyl iron-doped Ag/mesoporous carbon nanocomposites, carbon coil-carbon fiber hybrid materials and multiwalled CNTs/ZnO [38-40], the obtained CNS sample is also apt for microwave absorption.

As described in Table 1, when acetylene was decomposed over the No. 2 catalyst, compared to that of sample A, one can find that the yield of carbon materials at this case enhances greatly, and the yield is up to 309. Figure 6 depicts the FE-SEM images of the obtained sample B. As shown in Figure 6a, one can find that the majority of sample B is uniform CNSs (average size: 400 nm) and the content of these CNSs is up to 98%. A closer FE-SEM observation (as shown in Figure 6b) indicates that the obtained CNS connects with each other to form chain-like CNSs. Compared with that of sample A, the size of the obtained CNSs becomes small. Overall, the content of SnO_2 has a greatly impact on the yield and size of the obtained sample.

Figure 7 shows the EM spectra of Composite B. As illustrated in Figure 7a, the values of ε' are bigger than those of ε''. With an increasing frequency, the ε' and ε'' of the composite exhibit a fall from 22.33 to 13.52, and 12.20 to 7.33, respectively. The μ' and μ'' of the composite (as shown in Figure 7b) are almost constant ($\mu' \approx 1.0, \mu'' \approx 0$) in the frequency range of 2-18 GHz, which indicates the intrinsically small magnetic loss tangent. Figure 7c gives the $\tan\delta_E$ and $\tan\delta_m$ of the composite dependent on the frequency. It is apparent that the $\tan\delta_E$ values are much larger than those of $\tan\delta_m$, which confirms further that the dielectric loss plays the main role in the EM absorption. Moreover, one can observe clearly that the change trend of $\tan\delta_E$ inverses to that of $\tan\delta_m$. Such complementarities are effective for the strong EM attenuation, which implies that the obtained CNS sample has excellent EM absorption properties.

Figure 8 shows the typical relationship between RL and frequency of Composite B. Figure 8a indicates that the optimal absorption value of Composite B with a thickness of 1.5 mm is -20.4 dB at 13.0 GHz, which corresponds to 99% absorption. As shown in Figure 8b, the RL value below -5 dB (75% of EM wave attenuation) can be obtained in the whole frequency range, and RL value below -10 dB can be obtained in the 2.9-18 GHz frequency range. Compared to that of Composite A, Composite B exhibits an enhanced microwave absorbing properties.

As described in experiment, average 2.186 g of carbon species could be collected over the No. 3 catalyst. Compared to those of CNMs reported elsewhere [41], the obtained yield at this case enhances greatly. Figure 9 shows the FE-SEM images of sample C. Similar to those of samples A and B, uniform chain-like CNSs is the majority in the obtained sample, and the content of these structure is ca. 98%. The closer examination (as shown in Figure 9b) indicates the average size of the obtained uniform CNSs is ca. 180 nm, which is smaller than those of samples A and B. It is well known that the size of the obtained CNMs depends on the dimension of the used catalyst in CCVD process [41-44]. Therefore, one can find the size of the obtained CNSs decreases with the increasing content of SnO_2. In general, as shown in Table 2, the SnO_2 content has a great impact on the yield and size of the obtained sample.

The permittivity and permeability spectra, dielectric and magnetic loss, attenuation constant as a function of frequency for Composite C are shown in Figure 10. As illustrated in Figure 10a, the value of ε' decreases from 12.18 to 10.14, and the ε'' almost remains constant ($\varepsilon'' \approx 3.02$) in the whole frequency. Similar to those of Composites A and B, the μ' and μ'' of composite (as shown in Figure 10b) are almost constant ($\mu' \approx 1.05, \mu'' \approx 0.05$) in the frequency range of 2-18 GHz, the values of $\tan\delta_E$ are much larger than those of $\tan\delta_m$ (as shown in Figure 10c), and good complementarities can be observed between $\tan\delta_E$ and $\tan\delta_m$. According to the Eqs. (3), the attenuation constant of composites can be obtained, and the result is shown in Figure 10d. Compared to those of carbon nanocomposites reported before [45,46], the obtained Compsites (A, B and C) have the higher α values, indicating the excellent attenuation or microwave absorption.

Figure 11 shows the frequency dependence of RL results for Composite C. The results of Figure 11a indicates that the maximum RL value reaches -16.9 dB at 6.6 GHz with a d_m=3.5 mm. As shown in Figure 11b, the RL value below -10 dB can be obtained in the whole frequency range with the sample thickness varied from 1.2 to 10.0 mm. Importantly, double absorption feature (RL value below -10 dB) can be observed clearly in the thickness range of 4.0-10.0 mm, which is helpful for bandwidth broadening of microwave absorption. As shown in Table 3, the Composites B and C are superior to that of Composite A in microwave absorption. And our studies indicate that the chain-like CNSs also may have potential applications in the field of light weight microwave absorption materials.

3.3 Effect of SnO_2 and possible formation mechanism of CNSs.

As discussed above, the content of SnO_2 in catalyst can influence the yield and size of the obtained sample. However, as shown in Table 1, the yield of sample C is lower than those of samples A and B. As we all know that the small size can improve the catalytic ability of the catalyst effectively. Therefore, higher yield of CNSs should be obtained over the smaller size of the catalyst, which is not fully same to our obtained results. In order to understand the result, the microstructures of the as-synthesized catalysts were studied in detail. Figure 12 shows the microstructures and sizes of the obtained catalysts. As shown in Figure 12a, a typical TEM image of the No. 2 catalyst indicates that the obtained catalysts are core/shell structured Fe/SnO_2. The dimensions of shell and core are given in Figure 12b. One can find that the thickness of SnO_2 shell increases and the size of Fe core decreases with the enhancement of tin content. As reported by Liu et al. on $FeNi_3/Al_2O_3$ core/shell nanocomposites [22], the core particles with thicker shell are obviously smaller in size than those with thinner shell, which can also be confirmed further by our work. Although the small size of the catalyst is beneficial to

obtain high yield of CNCs, the thick SnO_2 shell weaken the catalytic ability of Fe particles to catalytically grow CNMs. Therefore, the competition between the core and shell substances leads that the highest CNS yield can be obtained over the No. 2 catalyst in this work.

In order to understand the possible formation mechanism of CNSs and the effect of SnO_2 further, A series of comparison experiments were designed and conducted: (i) the decomposition of acetylene was conducted at 700 °C without using any catalyst; (ii) the decomposition of acetylene was conducted at 700 °C over Fe nanoparticles generated by a combined sol-gel and reduction method; (iii) the decomposition of acetylene was conducted at 500 °C over the as-synthesized No. 1 catalyst. Figure 13 gives the FE-SEM images of the obtained samples. As shown in Figures 13a and b, the TEM and FE-SEM investigations indicate that the obtained samples at the cases (i) and (ii) are the mainly CNTs, CNTs and helical CNTs, respectively. And CNFs and helical CNFs are the majority in the obtained sample at the case (iii). One cannot find the presence of CNSs in the obtained samples at these cases, which indicates that the introduction of Sn into the catalyst and high decomposition temperature has a great impact on the formation of CNSs. Although the exact formation mechanism is still unclear, based on the obtained experimental results and models reported before [47-49], the theoretical model proposed by Gamaly and Ebbesen can explain the growth of CNSs under the adopted conditions effectively [49]. According to this model, the distribution velocity of carbon atoms on the surface of catalysts has a great impact on the growth of CNMs. And the mobility of surface carbon atoms is governed by the nature of catalyst, temperature, etc. The carbon atoms with the different distribution velocities can assemble into hexagonal, pentagonal and heptagonal rings. In the past years, as we all know that many theoretical studies revealed that pentagonal and heptagonal carbon rings were crucial for the formation of HCNMs and CNSs [50-52], and so many experimental results indicated that the addition of Sn into the Fe-group catalysts could improve the selectivity of HCNMs greatly [53-55]. Combined the reported theoretical and experimental results, one can find that the addition of Sn into the Fe-group catalysts is effective for carbon atoms to assemble into pentagonal and/or heptagonal rings, which can also be confirmed by our experimental results. Therefore, in our experiments, subject to the influence of the Fe/SnO_2 catalyst and high temperature, the carbon atoms generated on the catalyst surface assemble into pentagonal and/or heptagonal rings. The introduction of pentagonal and/or heptagonal carbon rings change in the curvature of graphitic flake, which induces the formation of CNSs [4,50]. However, because of the complexity of the synthesis processes, the exact growth mechanism of CNMs is still hot and controversial topic, and further research is needed to explain of the CNS growth mechanism.

4. Conclusions

In summary, high purity CNSs could be synthesized in ultrahigh yield over Fe/SnO_2 nanoparticles. The results demonstrated that the SnO_2 content in the catalyst had a great impact on the yield, dimension and microwave absorbing properties of the obtained sample. The ultrahigh yield of 309 was not reported before. Because of the better complementarities between $\tan\delta_E$ and $\tan\delta_m$, the smaller size chain-like CNSs exhibit enhanced microwave absorption properties. A possible mechanism was provided to understand the formation of CNSs. Therefore, a simple and environment-friendly route has been proposed for the synthesis of high purity chain-like CNSs in ultrahigh yield, and the as-synthesized chain-like CNSs may have potential applications as the light weight microwave absorption materials.

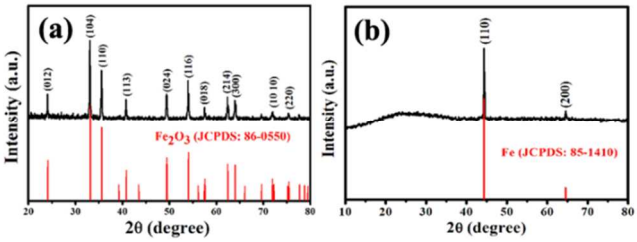

Figure 1. XRD patterns of the as-synthesized No. 1: (a) catalyst precursor, and (b) catalyst.

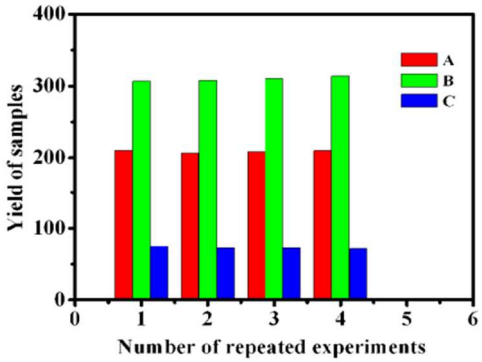

Figure 2. The statistical yields of the obtained samples in four separate runs.

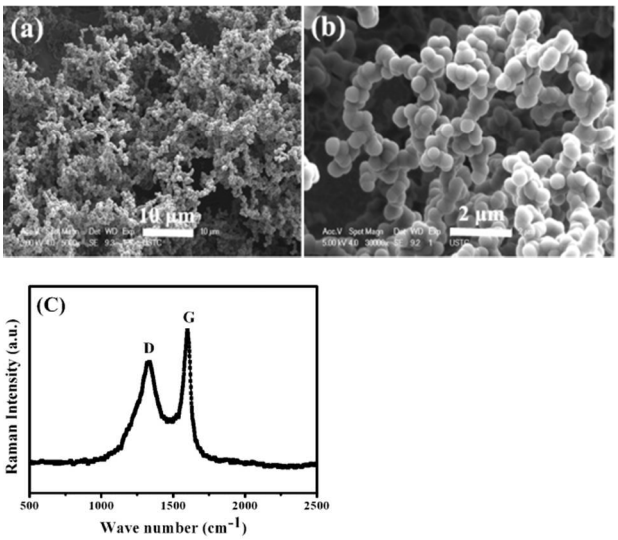

Figure 3. (a,b) Low and high magnification FE-SEM images, and (c) Raman spectrum of sample A.

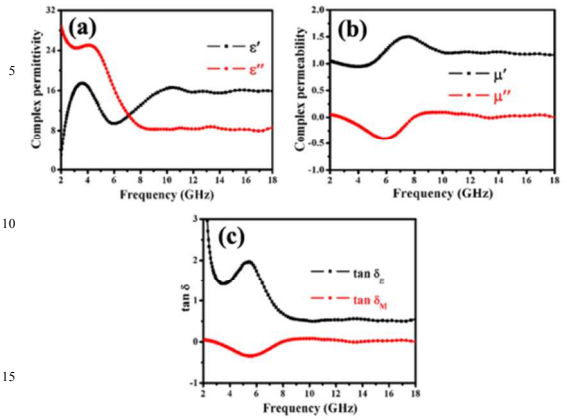

Figure 4. (a) Complex permittivity, (b) complex permeability, and (c) loss tangent as a function of frequency for Composite A.

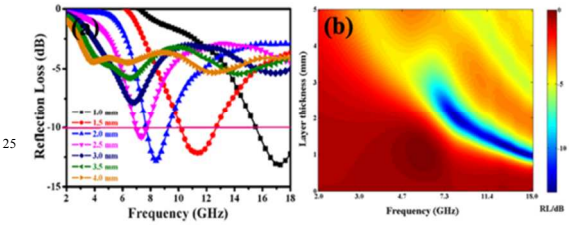

Figure 5. (a) RL versus frequency, and (b) Colour map of the RL values calculated from the measured EM parameters for Composite A.

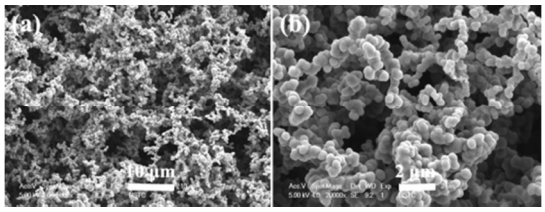

Figure 6. (a) Low, and (b) high magnification FE-SEM images of sample B.

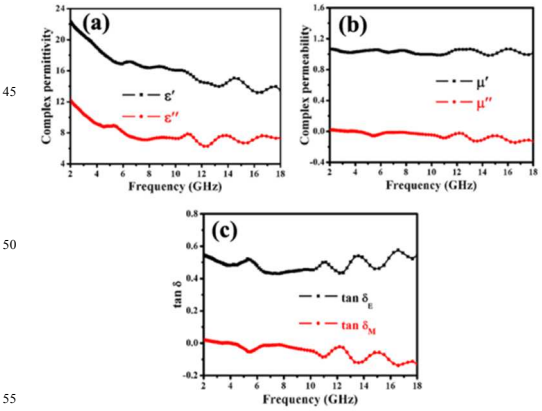

Figure 7. (a,b) EM parameters, and (c) loss tangent as a function of frequency for the Composite B.

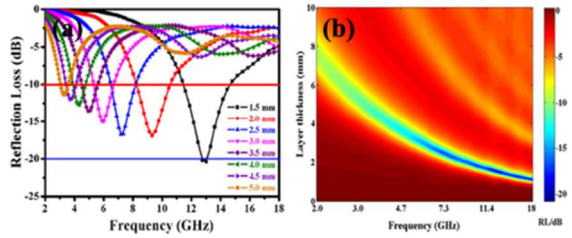

Figure 8. (a) RL value, and (b) two-dimensional representation of RL value as a function of frequency for Composite B.

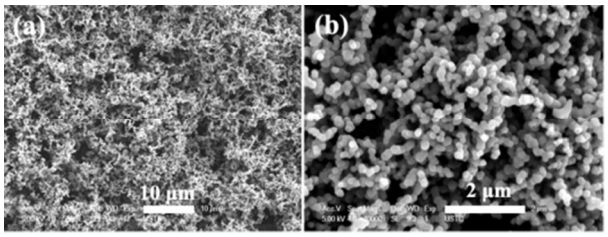

Figure 9. FE-SEM images of sample C: (a) low, and (b) high magnification.

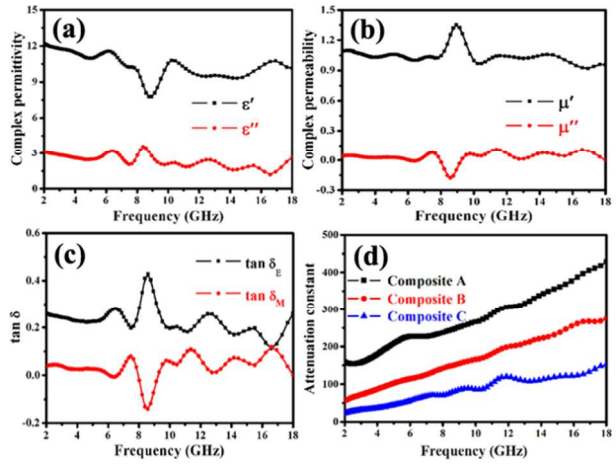

Figure 10. Frequency dependence of (a) complex permittivity, (b) complex permeability, (c) loss tangent, and (d) attenuation constant versus frequency of Composite C.

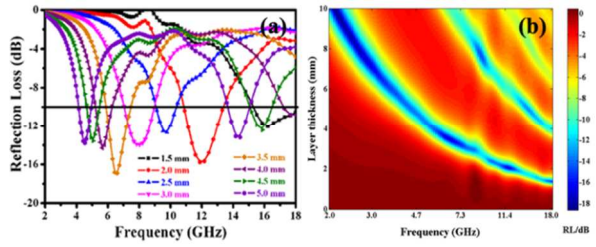

Figure 11. (a) RL versus frequency of Composite C, and (b) Colour map of the RL values calculated from the measured EM parameters.

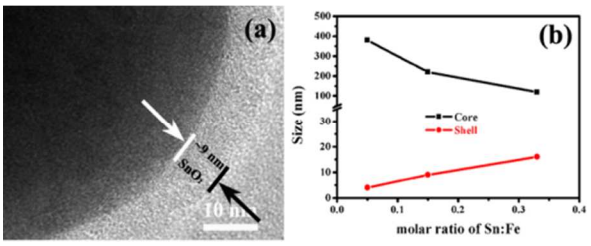

Figure 12. (a) A typical TEM image of the No.2 catalyst, and (b) average grain size of core and shell as a function of Sn molar concentration.

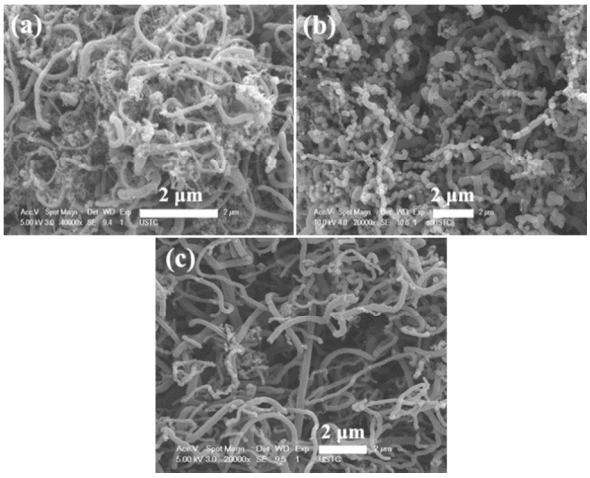

Figure 13. FE-SEM images of the samples obtained: (a) without using any catalyst at 700 °C, (b) over Fe nanoparticles at 700 °C, and (c) over No. 1 catalyst at 500 °C.

Table 1. The dependence of SnO_2 content in catalyst on the yield of the obtained sample.

Sample	Catalyst	Weight (g)	Yield (= $\frac{m_{total}}{m_{catalyst\ precursor}}$)
A	No. 1	6.260	209
B	No. 2	9.284	309
C	No. 3	2.186	73

Table 2. The dependence of SnO_2 on the CNS growth.

Catalyst	Molar ratio of Sn:Fe in catalyst	Yield	FE-SEM studies	Average size of sample (nm)
No. 1	1/20	209	Chain-like CNSs	500
No. 2	3/20	309	Chain-like CNSs	400
No. 3	1/3	73	Chain-like CNSs	180

Table 3. EM wave absorption properties of the representative chain-like CNSs.

Sample	Optical RL value (dB)	d_m (mm) (RL<-10dB)	Frequency range (RL<-10 dB)	Double absorption Peaks (RL<-10 dB)
A	-12.8	0.8-2.5	6.9-18 GHz	No
B	-20.4	1.2-5.0	2.9-18 GHz	No
C	-16.9	1.2-10.0	2-18 GHz	Yes

Acknowledgments

This work was supported by the International Cooperation Project of Guizhou Province (2012-7002), the National Science Foundation of Guizhou province (2014-2059), the National Science Foundation of China (Grant No. 11364005 and 11174132), and the Foundation of the National Key Project for Basic Research (2012CB9323402 and 2011CB922102) for financial support.

Notes and references

[a]*Physics Department, Guizhou University, Guiyang 550025, People's Republic of China*
[b]*Nanjing National Laboratory of Microstructures and Jiangsu Provincial Laboratory for NanoTechnology, Nanjing University, Nanjing 210093, People's Republic of China*
Fax: +86-25-83595535; Tel: +86-25-83621200;
E-mail: wzhong@nju.edu.cn

1 S. Iijima, Nature 1991, **354**, 56.
2 S. Yang, X. Chen and S. Motojima, Diam. Relat. Mater., 2004, 13, 2152.
3 H.W. Kroto, J.R. Heath, S.C. O'Brien, R.F. Curl and R.E. Smalley, Nature 1985, **318**, 162.
4 A. Nieto-Márquez, R. Romero, A. Romero and J.L. Valverde, J. Mater. Chem., 2011, **21**, 1664.
5 L. Tosheva, J. Parmentier, V. Valtchev, C. Vix-Guterl and J. Patarin, Carbon, 2005, **43**, 2474.
6 Y.D. Xia and R. Mokaya, Adv. Mater., 2004, **16**, 1553.
7 K.T. Lee, J.C. Lytle, N.S. Ergang, S.M. Oh and A. Stein, Adv. Funct.Mater., 2005, **15**, 547.
8 K.M. Pan, H. Ming, Y. Liu and Z.H. Kang. New J. Chem., 2012, **36**,113.
9 J.S. Qiu, Y.F. Li, Y.P. Wang, T.H. Wang, Z.B. Zhao, Y. Zhou, F. Li and H.M Cheng, Carbon 2003, **41**, 2170.
10 X. Xu, Z.Q. Li, D. Zhang and Z.X. Chen, Carbon 2011, **49**, 275.
11 W.R. Li, D.H. Chen, Z. Li, Y.F. Shi, Y. Wan, G. Wang, Z.Y. Jiang and D.Y. Zhao, Carbon 2007, **45**, 1757.
12 X.S. Qi, Q. Ding, W. Zhong, C.T. Au and Y.W. Du. Carbon 2013, **56**, 383.
13 B.L. Liu, W.C. Ren, C. Liu, C.H. Sun, L.B. Gao, S.S. Li, C.B. Jiang and H.M. Cheng, Acs. Nano., 2009, **3**, 3421.
14 G.F. Zhong, J.H. Warner, M. Fouquet, A.W. Robertson, B.G. Chen and J. Robertson, Acs. Nano., 2012, **6**, 2893.
15 F. Tian and C.N. He, Mater. Chem. Phys., 2010, **123**, 351.
16 Z. Mehraban, F. Farzaneh and V. Dadmehr. Mater. Lett., 2009, **63**, 1653.
17 X.C. Chen, H. Wang and J.H. He, Nanotechnology, 2008, **19**, 325607.
18 Z.J. Wang, L.N. Wu, J.G. Zhou, W. Cai, B.Z. Shen and Z.H. Jiang, J.Phys. Chem. C, 2013, **117**, 5446.
19 N. Li, C.W. Hu and M.H. Cao, Phys. Chem. Chem. Phys., 2013, **15**, 7685.
20 Y. Tang, Y. Shao, K.F. Yao and Y.X. Zhong Nanotechnology, 2014, **25**, 035704.
21 X.S. Qi, Y. Deng, W. Zhong, Y. Yang, C. Qin, C.T. Au and Y.W. Du, J. Phys. Chem. C, 2010, **114**, 808.
22 W. Liu, W. Zhong, H.Y. Jiang, N.J. Tang, X.L. Wu and Y.W. Du, Eur. Phys. J. B, 2005, **46**, 471.
23 H. Kaori and Y. Nakayama. Carbon, 2013, **56**, 264.
24 D.W. Li and L.J. Pan, J. Mater. Res., 2012, **27**, 431.
25 N. Okazaki, S. Hosokawa, T. Goto and Y. Nakayama, J. Phys. Chem.C, 2010, **114**, 808.
26 N.J. Tang, Y. Yang, K.J. Lin, W. Zhong, C.T. Au and Y.W. Du, J. Phys. Chem. C, 2008, **112**, 10061.
27 P. Serp, R. Feuer, P. Kalck, Y. Kihn, J. L. Faria and J.L. Figueiredo, Carbon, 2001, **39**, 621.
28 U. Ritter, P. Scharff, C. Siegmund, O.P. Dmytrenko, N.P. Kulish, Y.I. Prylutskyy, N.M Belyi, V.A. Gubanov, L.I. Komarova, S.V. Lizunova, V.G. Poroshin, V.V. Shlapatskaya and H. Bernas, Carbon, 2006, **44**, 2694.
29 U. Ritter, P. Scharff, O.P .Dmytrenko, N.P. Kulish, Y.I. Prylutskyy, N.M. Belyi, V.A. Gubanov, L.A. Komarova, S.V. Lizunova and V.V. Shlapatskaya, Chem. Phys. Lett., 2007, **447**, 252.
30 I. Abdull, N. Sakulchaicharoen and J.E. Herrera, Diam. Relat. Mater., 2012, **21**, 76.
31 D.W. Li, L.J. Pan, Y.K. Wu, and W. Peng , Carbon, 2013, **50**, 2571.
32 X.G. Liu, B. Li, D.Y. Gen, W.B. Cui, F. Yang and Z.G. Xie, Carbon, 2009, **47**, 470.
33 L.J. Deng and M.G. Han, Appl. Phys. Lett., 2007, **91**, 023119.
34 S.C. Chiu, H.C. Yu and Y.Y. Li, J. Phys. Chem. C., 2010, **114**, 1947.
35 C. Wang, X.J. Han, P. Xu, X.L. Zhang, Y.C. Du and S.R. Hu, Appl. Phys. Lett., 2012, **100**, 046102.
36 X.F. Zhang, P.F. Guan and X.L. Dong, Appl. Phys. Lett., 2010, **97**, 033107.
37 Y.P. Sun, X.G. Liu, C.G. Jin, A.L. Xia, S.S. Zhao, W.H. Li, C. Feng, F. Xiao and Y.X. Wu, RSC Adv., 2013, **3**, 18082.
38 H.J. Wu, L.D. Wang, Y.M. Wang, S.L. Guo and Z.Y. Shen, Mater. Sci. Eng. B, 2012, **177**, 476.
39 L. Liu, K.C. Zhou, P.G. He and T.F. Chen, Mater. Lett., 2013, 110, 76.
40 W.L. Song, M.S. Cao, B. Wen, Z.L. Hou, J. Cheng and J. Yuan, Mater. Res. Bull., 2012, **47**, 1747.
41 N.J. Tang, J.F. Wen, Y. Zhang, F.X. Liu, K.J. Lin and Y.W. Du, Acs Nano., 2010, **4**, 241.
42 B.L. Liu, W. Ren, L.B. Gao, S.S. Li, S.F. Pei, C. Liu, C.B. Jiang and H.M. Cheng, J. Am. Chem. Soc., 2009, **131**, 2082.
43 S.M. Huang, Q. Cai, J.Y. Chen, Y. Qian and L.J. Zhang, J. A. Chem. Soc., 2009, **131**, 2094.
44 A. Hirsch, Angew. Chem. Int. Ed., 2009, **48**, 5403.
45 F.S. Wen, F. Zhang and Z.Y. Liu, J. Phys. Chem. C., 2011, **115**, 14025.
46 B. Lu, H. Huang, X.L. Dong, X.F. Zhang, J.P. Lei, J.P. Sun and C. Dong, J. Appl. Phys., 2008, **104**, 114313.
47 S. Amelickx, X.B. Zhang, D. Bernaerts, X.F. Zhang, V. Ivanov and J.B. Nagy, Science, 1995, **267**, 635.
48 S. Fan, M.G. Chapline, N.R. Franklin, T.W. Tombler, A.M. Cassell and H. Dai, Science, 1999, **283**, 512.
49 E.G. Gamaly and T.W. Ebbesen, Phys. Rev., 1995, **52**, 2083.
50 Z.C. Kang and Z.L. Wang, J. Phys. Chem., 1996, **100**, 5163.
51 S. Itoh, S. Ihara and J. Kitakami, Phys. Rev. B, 1993, **47**, 1703.
52 H.Q. Hou, Z. Jun, F. Weller and A. Greiner, Chem. Mater., 2003, **15**, 3170.
53 W. Wang, K.Q. Yang, J. Gaillard, P.R. Bandaru and A.M. Rao, Adv. Mater., 2008, **20**, 179.
54 D.W. Li, L.J. Pan, Y.K. Wu and W. Peng, Carbon, 2012, **50**, 2571.
55 K. Hirahara and Y. Nakayama, Carbon, 2013, **56**, 264.